Received: 22 April 2022 | Revised: 3 September 2022 | Accepted: 6 September 2022

DOI: 10.1002/elps.202200102

ELECTROPHORESIS

RESEARCH ARTICLE

The electrodynamics of rod-like microparticles based on optically induced dielectrophoresis

Liuyong Shi[1] | **Xiangtao Zhong**[1] | **Tao Wu**[1] | **Qin Bian**[1] | **Xiaomei Liu**[1] | **Huaqing Miao**[2] | **Yongbo Deng**[3] | **Binfeng Yin**[4] | **Teng Zhou**[1]

[1]Mechanical and Electrical Engineering College, Hainan University, Haikou, P. R. China

[2]Shenzhen Academy of Metrology & Quality Inspection, Shenzhen, P. R. China

[3]Changchun Institute of Optics, Fine Mechanics and Physics (CIOMP), Chinese Academy of Science, Changchun, P. R. China

[4]School of Mechanical Engineering, Yangzhou University, Yangzhou, P. R. China

Correspondence
Teng Zhou, Mechanical and Electrical Engineering College, Hainan University, No 58, Renmin Avenue, Haikou 570228, Hainan province, P. R. China.
Email: zhouteng@hainanu.edu.cn

Color online: See article online to view Figures 1–5 in color.

Funding information
Hainan Province Science and Technology Special Fund, Grant/Award Number: ZDYF2022SHFZ033; National Natural Science Foundation of China, Grant/Award Numbers: 61964006, 52075138; Natural Science Foundation of Jiangsu Province, Grant/Award Number: BK20190872

Abstract

Due to its characteristics of noncontact, non-damage, high flux, and easy-to-achieve flexible manipulation, optically induced dielectrophoresis (ODEP) technology has been employed to manipulate microspherical biological particles, including separation, enrichment, capture, arrangement, and fusion. However, in nature, biomolecules are morphologically diverse, and some of them are rod-like. In order to illustrate the electrodynamics of rodlike particles under the action of ODEP, a transient multi-physical field coupling model of ODEP chip under the hypothesis of electrical double layer thin layer was established in this paper. The arbitrary Lagrangian–Eulerian method is used to track single-rod particle in the strong coupled flow field and electric field simultaneously. The influence of several key factors, including the applied alternating current (AC) electric voltage, the width of optical bright area, and the initial position of particle, on the trajectory of particle center was analyzed in positive dielectrophoresis (DEP) action and negative DEP action, respectively. Especially, the planar motion process of rodlike particles was discussed together. The research results reveal the electrodynamics behavior of rodlike particles based on the action of ODEP, which may provide theoretical support for the further design of rodlike biological cells manipulation chip based on AC ODEP technology in the future.

KEYWORDS

arbitrary Lagrangian–Eulerian, electrodynamics, microfluidic, optically induced dielectrophoresis, rodlike particles

1 | INTRODUCTION

Biological cell manipulation technology, such as the separation, capture, and detection of biological particles [1–3], including tumor cells [4–6] and DNA molecules [7–9], has become a research hot spot in biomedical field. Microfluidic chip, also known as lab-on-a-chip or micro total analysis system, has the advantages of small size, low cost, low consumption of samples and reagents, and so on, so it is especially suitable for biological applications. Compared with other manipulation techniques, such as atomic force microscope [10, 11], microneedle [12, 13], acoustic trap [14, 15], optical tweezers [16, 17], and magnetic tweezers [18–20], the dielectrophoresis (DEP) microfluidic chip

Abbreviations: AC, alternating current; ALE, arbitrary Lagrangian–Eulerian; DEP, dielectrophoresis; ITO, indium tin oxide; MST, Maxwell stress tensor; ODEP, optically induced dielectrophoresis.

[21, 22], as a micro–nano manipulation technology that is easy to integrate and control, can realize the manipulation of single or large quantities of particles [23–28] due to the characteristics of noncontact, non-damage, and high flux. However, traditional electrophoretic technology requires the design and processing of complex physical electrodes, which causes the problems of high cost and long design cycle inevitably. Meantime, the flexibility of the electrophoretic chip is limited by fixed structure electrodes.

The optically induced dielectrophoresis (ODEP) technology is combined with a virtual electrode defined by light irradiating on the photoconductive materials to generate a nonuniform electric field to realize the manipulation of cells [29, 30]. Compared to traditional electrophoretic techniques, ODEP discards the preparation of expensive metal electrode structures, and it uses advanced digital micromirror device to write the designed electrode patterns into a photoconductive material to mimic physical electrode [31, 32], so called optical virtual electrode. Based on the real-time reconfigured optical virtual electrode, flexible manipulation mode can be achieved, which is not available in traditional electrophoretic techniques. In recent years, ODEP has been more and more widely employed in microfluidic chip, and the manipulation and assembly of polystyrene spheres [33, 34], cancer cells [35, 36], bacteria [37, 38], and even drug-containing particles [39, 40] have been realized based on ODEP technology. However, previous studies on ODEP technology are usually focused on the manipulation of spherical particles. In nature, biomolecules are morphologically diverse, and some take on other shapes, such as rodlike. The research on the electrodynamics behavior of rodlike particles under the action of ODEP is conducive to expand its application in biomedical field.

In this study, based on the structural characteristics of the ODEP microfluidic chip, the transient numerical model containing rodlike microparticle is established in the strong coupled electric–fluid–solid field. The time-average alternating current (AC) DEP force and fluid viscosity resistance acting on particles are calculated by the Maxwell stress tensor (MST), which is proved to be the most rigorous method for calculating DEP force and can be used to explain the electric field distortion induced by the presence of particles [41, 42]. The arbitrary Lagrangian–Eulerian (ALE) method is used for numerical solution, which employs the Lagrange approach tracing particles combined with the Euler method to describe the flow field, especially suitable for processing the grid distortion [43, 44]. The planar motion process of rodlike particles is illustrated; further, the influences of several crucial factors, including applied AC electric voltage, optical bright area width, and initial position of particle on particle trajectory, are discussed in both positive and negative DEP cases, respectively.

2 | NUMERICAL MODEL CONSTRUCTION AND IMPLEMENTATION

2.1 | Numerical model construction

The ODEP chip is generally assembled into a three-layered structure: Indium tin oxide (ITO) conductive glass in the upper layer, SU-8 spacer in the middle, and photoconductivity layer in the lower layer, in which the photoconductivity layer is a multilayered structure deposited on transparent ITO glass, from bottom to top: heavily doped hydrogenated amorphous silicon ($n^+\alpha$-Si:H) layer for reducing the contact resistance between the substrate and intrinsic hydrogenated amorphous silicon (α-Si:H) layer (forming a photoconductive reaction area) and nitride insulation layer (preventing hydrolysis at low frequency and high potential) [29]. In this study, the whole model is treated as a two-dimensional (2D) structure for simplifying calculation. As shown in Figure 1, the rodlike particle, composed of two semicircles with diametral d_2 at both ends and a rectangle with length d_1 and width d_2 in the middle, moves within a rectangular microchannel CDEF filled with fluid medium, where the height of the rectangular microchannel CDEF is H and the length is L. A 2D rectangular coordinate system is established with the symmetry center of the rectangular microchannel CDEF. An alternating voltage is applied to the top boundary cyclodextrin and the bottom boundary AB of the modeled thin membrane electrodes. The brown area ABEF under the rectangular microchannel represents the photoconductive layer with a width h and a length L. Because of the light source illumination at the bottom of the microchannel, two optically bright regions with a diameter of d_L are generated in the photoconductive layer ABEF.

The specific geometric parameters of the microchannel are set as follows: microchannel length $L = 200$ μm, height $H = 100$ μm. The thickness of the photoconductivity layer made of intrinsic amorphous silicon is $h = 2$ μm. The rodlike particles are composed of a semicircle with a diameter of $d_2 = 5$ μm and a rectangle with a length of $d_1 = 20$ μm and a width of d_2. The width of bright area is $d_L = 30$ μm. The rectangular microchannel is filled with deionized aqueous solution with its density $\rho_F = 1 \times 10^3$ kg/m^3, dynamic viscosity $\mu = 1 \times 10^{-3}$ Pa s, conductivity $\sigma_F = 1 \times 10^{-3}$ S/m, and relative dielectric constant $\varepsilon_F = 80$ as the fluid medium. The polystyrene particle density is $\rho_P = 1.05 \times 10^3$ S/m, the shear modulus is $G_P = 1 \times 10^9$ Pa, and the relative

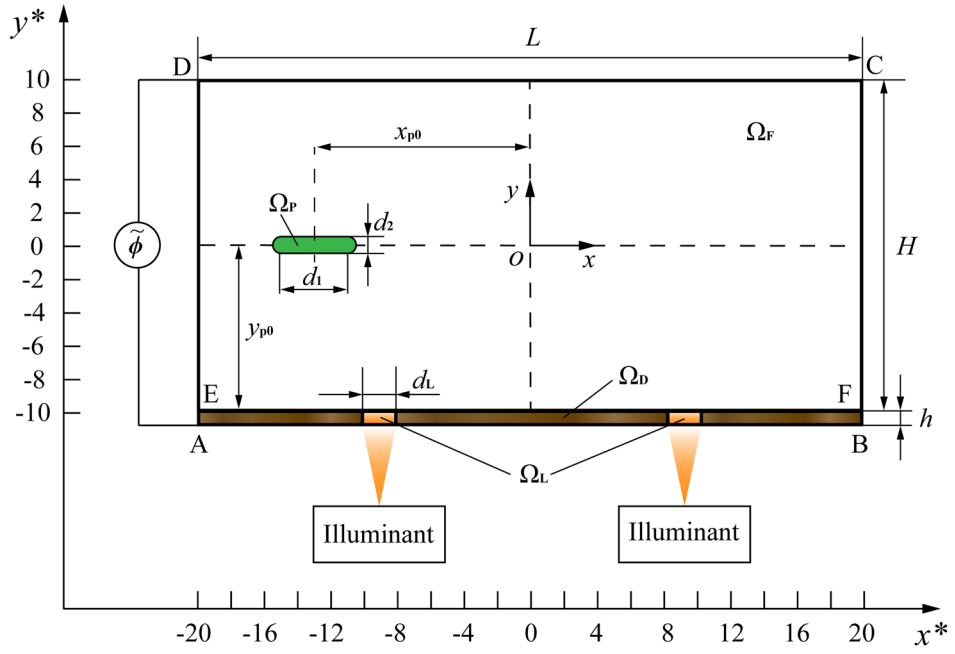

FIGURE 1 The two-dimensional (2D) schematic diagram of the optically induced dielectrophoresis (ODEP) chip, including a single-rod-like particle into a rectangular microchannel structure. The origin of the XOY 2D plane coordinate system is located at the center of the rectangular microchannel. The coordinate system (x^*, y^*) is the dimensionless result of applying the characteristic length to the original coordinate system (x, y). The green rod represents microparticle. The photoconductive layer in the microchannel is represented by the orange and brown color blocks, where the orange area is the illuminated area (bright area), and the remaining colorless and brown areas are the unilluminated areas (dark area). Ω_P, Ω_F, Ω_L, and $\Omega_D$represent the particle domain (the green rod area), the fluid medium domain (corresponds to the region CDEF), and the bright and dark domains (the region ABFE), respectively.

permittivity is $\varepsilon_P = 2.6$. The electrical conductivities of particles $\sigma_{P1} = 4 \times 10^{-2}$ S/m and $\sigma_{P2} = 4 \times 10^{-4}$ S/m are selected to generate positive and negative DEP actions, respectively. The relative permittivity of the photoconductivity layer is $\varepsilon_S = 11.7$, the conductivity of the bright region is $\sigma_L = 2 \times 10^{-1}$ S/m, and the conductivity of the dark region is $\sigma_D = 6.7 \times 10^{-5}$ S/m. The frequency of the applied AC electric field is $f = 1$ MHz, and the peak voltage is $\phi_0 = 30$ V.

2.2 | Numerical model implementation

Corresponding to the previous numerical model, the complete governing equations and boundary conditions are presented in Section S1. Then, the designed model was implemented and solved with the aid of four classic built-in physics modules in COMSOL (version 5.5, COMSOL Group, Stockholm, Sweden): solid mechanics, moving mesh, laminar flow, and electric current. Our previous work, including dielectrophoresis phenomenon of particles in a converging-diverging microchannel [45, 46], DEP interaction in an AC electric field [47, 48], the electrodynamics of rigid particles in ODEP chip [49], and the continuous separation of microparticles based on ODEP [50], has proved the accuracy and reliability of this method.

3 | RESULTS AND DISCUSSION

3.1 | The distribution of electric field

Figure 2 shows the electric field intensity distribution when the particle is located at its different positions. It can be seen from Figure 2 that a strong nonuniform electric field is formed around the bright areas where the light illuminates the photoconductive material layer. The electric field intensity at the junction of the bright area and the dark area is more significant than that of other areas (including the center of the bright areas and the area far from the bright areas). The presence of particles will also disturb their surrounding electric field to a certain extent. By comparing Figure 2A,C, the particle with the electrical conductivity of $\sigma_P = 4 \times 10^{-2}$ S/m is attracted to the left one of the bright areas with high electric field intensity under the action of DEP force, namely, the positive DEP action, and a weak electric field is formed inside the particle. On the contrary, as shown in Figure 2B,D, the particle with a conductivity of $\sigma_P = 4 \times 10^{-4}$ S/m will be repulsed to the

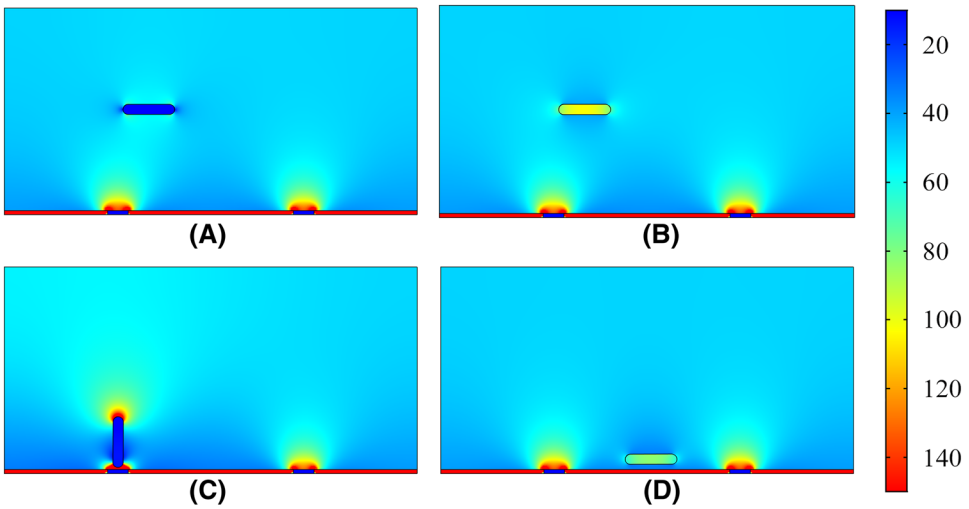

FIGURE 2 The distribution of the electric field intensity when the particle locates at its different positions. $\tilde{\phi} = 30$ V, $d_L = 10$ μm, $(x^*_{p0}, y^*_{p0}) = (-6,0)$, the particle conductivity in (A and C) is $\sigma_P = 4 \times 10^{-2}$ S/m, whereas $\sigma_P = 4 \times 10^{-4}$ S/m in (B and D). Here, the rod represents the particle, the color legend represents the electric field intensity, and the arrows represent the electric field direction.

center of the bright areas with low electric field intensity, which is negative DEP force action, and a strong electric field is formed inside the particle.

When the particle is immersed into the nonuniform electric field, the DEP force acting particle is dominated by the real part of the Clausius–Mossotti (CM) factor, $K(\omega)$,which depends on the complex permittivity of the particle and the fluid media:

$$K(\omega) = \frac{\widetilde{\varepsilon_P} - \widetilde{\varepsilon_F}}{\widetilde{\varepsilon_P} + 2\widetilde{\varepsilon_F}} \quad (1)$$

where $\widetilde{\varepsilon_P}$ and $\widetilde{\varepsilon_F}$ represent the complex permittivity of particles and fluid media, respectively, and $\widetilde{\varepsilon} = \varepsilon - i\sigma/\omega$, ε represents permittivity.

Based on the parameters employed in this model, the calculation results from Equation (1) show the real part of the CM factor with the particle conductivity of $\sigma_P = 4 \times 10^{-2}$ and 4×10^{-4} S/m equal to 0.8663 and −0.4612, respectively; thus, the particle with conductivity 4×10^{-2} S/m will be subjected to the positive DEP action and attracted to strong electric field areas, the other will be subjected to the negative DEP action and repelled to weak electric field area (Movies S1 and S2), which is consistent with the conclusions of some literatures [51, 52].

3.2 | The planar motion of the particle

Considering that the rodlike particle is regarded as a 2D rigid body, its electrodynamic behavior in this model can be regarded as a planar motion, including translation and rotation. For the particle with $\sigma_P = 4 \times 10^{-2}$ S/m, particle orientation and DEP force distribution on its surface at different times are exhibited in Figure 3. It can be seen from Figure 3A, after the particle departs, the particle keeps rotating counterclockwise until it reaches the vertical orientation. After that, it will stop rotating and begin to translate, and its vertical orientation will remain the same for a while until the particle finally translates to the left one of the bright areas. It can be seen from Figure 3B,C that almost antisymmetric DEP forces are generated on the particle surface, but they cannot completely offset each other; a resultant force couple is created to force the particle to rotate. In Figure 3D, when the particle translates to right above the bright area, the DEP force from the nonuniform electric field around the bright area is symmetrically distributed in the horizontal direction; thus, the x component of DEP force is removed. Simultaneously, the nonuniform electric field around another optical spot is far away from the particle and has little effect on it, almost the y component of DEP force remains, so the particle keeps translating and finally moves to the left optical bright area with a vertical orientation.

As for the particle with a conductivity $\sigma_P = 4 \times 10^{-4}$ S/m, the particle orientation and DEP force distribution at different times are shown in Figure 4. In contrast to those shown in Figure 3, the particle almost keeps rotating clockwise until it eventually moves to the middle area between the two bright areas with the horizontal orientation as shown in Figure 4A. When the particle deviates to one of the optical spots, an antisymmetric DEP force distribution is formed on the surface of the particle in Figure 4B,C, and a resultant force couple is generated to force the particle to rotate continuously. When the particle reaches the middle position of the two bright areas, the symmetrically

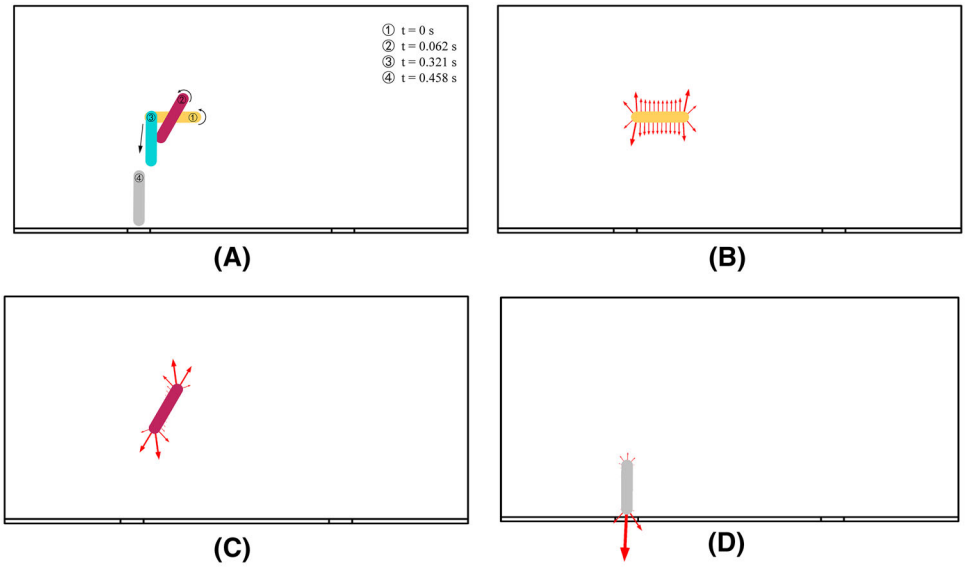

FIGURE 3 Particle orientation (A) and dielectrophoresis (DEP) force distribution of at different times with $\sigma_P = 4 \times 10^{-2}$ S/m, $\tilde{\phi} = 30$ V, $d_L = 10$ μm, $(x^*_{p0}, y^*_{p0}) = (-6,0)$. (B) $t = 0$ s, (C) $t = 0.062$ s, and (D) $t = 0.458$ s. The direction and length of the arrows represent the magnitude and direction of the DEP force.

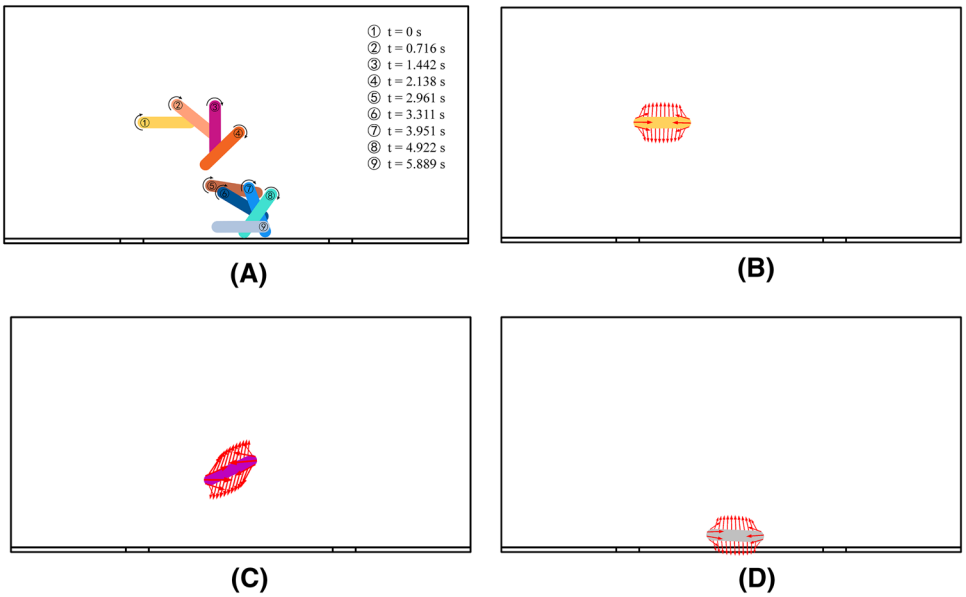

FIGURE 4 Particle orientation (A) and dielectrophoresis (DEP) force distribution of at different times with $\sigma_P = 4 \times 10^{-4}$ S/m, $\tilde{\phi} = 30$ V, $d_L = 10$ μm, $(x^*_{p0}, y^*_{p0}) = (-6,0)$. (B) $t = 0$ s, (C) $t = 2.431$ s, and (D) $t = 5.589$ s. The direction and length of the arrows represent the magnitude and direction of the DEP force.

distributed DEP force is produced on the surface of the particle in Figure 4D, so the particle achieves an equilibrium position with a horizontal orientation. Compared with Figure 3, the particle in Figure 4 needs more than 10 times longer time to reach its destination. With little difference in path length, the particle with positive DEP action should have higher translational speed.

3.3 | The trajectory of particle center point

The trajectory of particle center point reflects its electrodynamic behavior throughout, which is affected by some crucial parameters, including applied AC electric voltage, the width of optical bright area, and the initial position of

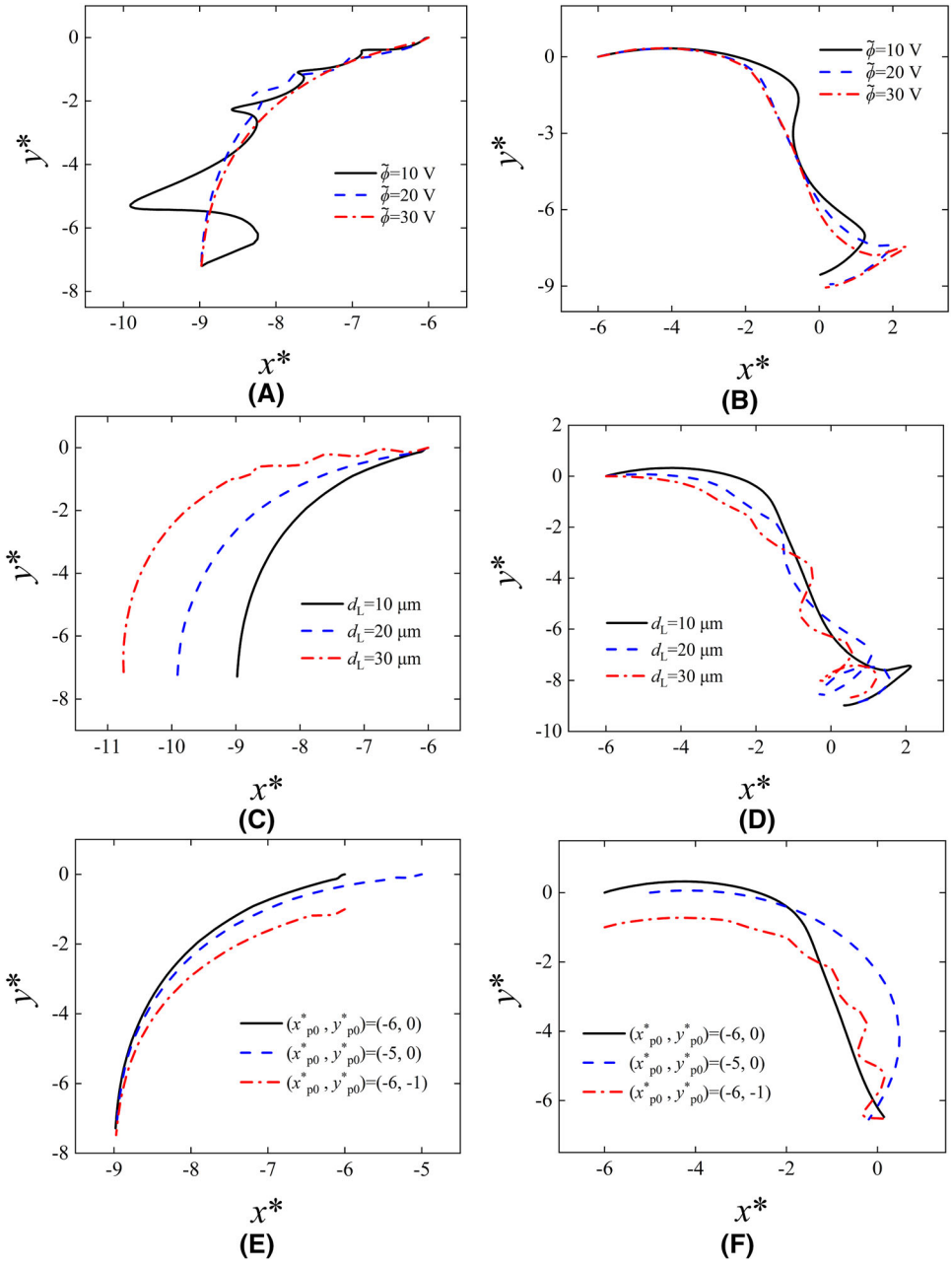

FIGURE 5 The trajectory of particle center point with the different applied alternating current (AC) electric voltages, the width of bright area, the initial position of particles. (A), (C), (E) The positive dielectrophoresis (DEP) action ($\sigma_P = 4{\times}10^{-2}$ S/m); (B), (D), (F) the negative DEP action ($\sigma_P = 4 \times 10^{-4}$ S/m)

particle so on, as shown in Figure 5. The parametric scanning method is adopted here, that is, when one parameter is changed, the other parameters remain identical.

As can be seen from Figure 5A, in the case of positive DEP action, when the applied AC voltage is 10 and 20 V, the trajectory of the particle center point resembles an oscillating curve, that means the center point of the particle moves left and right in the *x*-axis direction, which may be caused by the rotation of the particle. However, when the voltage is elevated to 30 V, the trajectory graph is relatively smooth. From Equation (12) of DEP force (see supplementary material S1), it can be known that the particle will undoubtedly experience greater DEP force at higher voltage; it will take less time for the throughout movement process of particle, so the oscillation amplitude of the trajectory curve is relatively weakened. In the case of negative DEP corresponding to Figure 5B, as the particles are located in the middle area of the two optical spots most of the time, the *x* components of DEP forces caused by the electric fields around the two optical spots are largely offset each other, so increasing the voltage has little effect on the particle trajectory. With the increasing width of the bright area, the

width of the dark area and the central point between the two bright areas remain identical at the same time, that is, it is still located at $x^* = 0$; thus, the bright area extends outwards. As shown in Figure 5C, the particle under the action of positive DEP will arrive at the updated position of bright areas. However, the particle under the action of negative DEP will still approach to the original central point of the two bright areas in Figure 5D. In Figure 5E,F, except for a short period of time at the beginning, the particles departing from different initial positions will be subjected to similar DEP force and liquid viscous resistance; thus, they experience almost identical particle trajectories. It should also be noted that, because of the size of the particle itself, the trajectory of its central point cannot eventually extend to the wall. Meanwhile, because the initial velocity of the fluid is set to zero, the Reynolds number of the model is relatively small, and the particle is away from the wall during most of the time, and the wall effect has little effect on the particle motion.

4 | CONCLUDING REMARKS

In this study, the transient multi-physical field coupling ODEP model under the assumption of an electrical double layer thin layer is established and solved. The MST is adopted to calculate the DEP force and liquid viscous resistance of particles. The ALE method is applied to trace the motion process of single-rod rigid particle in the strong coupled flow field and electric field. The planar motion process of rodlike particles is elucidated in detail, and the influence of several key parameters, including the applied AC electric voltage, the width of the bright area, and the initial position on the trajectory of particle center, is explained. The calculation results show that when the applied AC voltage is less than 30 V, the trajectory of the particle center point presents as an oscillating curve due to the rotation of the particle, when the voltage increases to 30 V, the trajectory becomes smooth. With the increasing width of the bright area, the particles affected by positive DEP action will move to the center of the updated bright area. In contrast, the destination of the particles affected by negative DEP action remains unchanged. The initial position of the particle has little effect on particle trajectory, but it will take different movement times for the particles. The ODEP model established in this study reasonably clarifies the electrodynamics behavior of rodlike particles under the action of ODEP and may provide theoretical support for the further design of real rodlike biological cells (*Escherichia coli*, filamentous microalgae, etc.) manipulation chips based on AC-ODEP technology in the future.

ACKNOWLEDGMENTS

This work is funded by Hainan Province Science and Technology Special Fund (Grant no. ZDYF2022SHFZ033), the National Natural Science Foundation of China (Grant nos. 61964006, 52075138), and the Natural Science Foundation of Jiangsu Province (Grant no. BK20190872).

CONFLICT OF INTEREST

The authors have declared no conflict of interest.

DATA AVAILABILITY STATEMENT

The data that support the findings of this study are available from the corresponding author upon reasonable request.

ORCID

Liuyong Shi https://orcid.org/0000-0002-1412-4237
Xiangtao Zhong https://orcid.org/0000-0003-1263-8856
Teng Zhou https://orcid.org/0000-0002-8744-9083

REFERENCES

1. Shoji S, Ohori T, Kawashima H, Miura K, Yotsumoto A. Mechanical micro flow control devices for medical and biomedical micro total analysis systems (mu TAS). Proc Electrochem Soc. 1997;97(5):12–9.
2. Yang R, Wu MX, Jin GF. An integrated micro optical and micro fluidic system for micro-total analysis system. Proc Soc Photo-Opt Instrum. 2000;4177:208–11.
3. Hou T, Chang H, Jiang H, Wang P, Li N, Song Y, et al. Smartphone based microfluidic lab-on-chip device for real-time detection, counting and sizing of living algae. Measurement. 2022;187:110304.
4. Liotta LA, Saidel MG, Kleinerman J. The significance of hematogenous tumor cell clumps in the metastatic process. Cancer Res. 1976;36(3):889–94.
5. Fox JL, Vu EN, Doyle-Waters M, Brubacher JR, Abu-Laban R, Hu ZX. Prophylactic hypothermia for traumatic brain injury: a quantitative systematic review. Can J Emerg Med. 2010;12(4):355–64.
6. Tang HR, Wang H, Yang C, Zhao DD, Qian YY, Li YX. Nanopore-based strategy for selective detection of single carcinoembryonic antigen (CEA) molecules. Anal Chem. 2020;92(4):3042–9.
7. Luan BQ, Stolovitzky G, Martyna G. Slowing and controlling the translocation of DNA in a solid-state nanopore. Nanoscale. 2012;4(4):1068–77.
8. Cheung KM, Abendroth JM, Nakatsuka N, Zhu BW, Yang Y, Andrews AM, et al. Detecting DNA and RNA and differentiating single-nucleotide variations via field-effect transistors. Nano Lett. 2020;20(8):5982–90.
9. Ding TL, Yang J, Pan V, Zhao N, Lu ZH, Ke YG, et al. DNA nanotechnology assisted nanopore-based analysis. Nucleic Acids Res. 2020;48(6):2791–806.
10. Cervantes NA, Gutierrez-Medina B. Robust deposition of lambda DNA on mica for imaging by AFM in air. Scanning. 2014;36(6):561–9.
11. Li H, Oberhauser AF, Redick SD, Carrion-Vazquez M, Erickson HP, Fernandez JM. Multiple conformations of PEVK proteins

detected by single-molecule techniques. Proc Natl Acad Sci USA. 2001;98(19):10682–6.
12. Held J, Gaspar J, Ruther P, Hagner M, Cismak A, Heilmann A, et al. Systematic characterization of DRIE-based fabrication process of silicon microneedles. Microelectromech Syst Mater Devices. 2008;1052:707.
13. Teo AL, Shearwood C, Ng KC, Lu J, Moochhala S. Transdermal microneedles for drug delivery applications. Mater Sci Eng B. 2006;132(1–2):151–4.
14. Kozuka T, Yasui K, Tuziuti T, Towata A, Ilda Y. Acoustic standing-wave field for manipulation in air. Jpn J Appl Phys. 2008;47(5):4336–8.
15. Hwang JY, Cheon DY, Shin H, Kim HB, Lee J. Near-field acoustic microbead trapping as remote anchor for single particle manipulation. Appl Phys Lett. 2015;106(18):183704.
16. Bzdek BR, Collard L, Sprittles JE, Hudson AJ, Reid JP. Dynamic measurements and simulations of airborne picolitre-droplet coalescence in holographic optical tweezers. J Chem Phys. 2016;145(5):054502.
17. Kim H, Lee W, Lee HG, Jo H, Song Y, Ahn J. *In situ* single-atom array synthesis using dynamic holographic optical tweezers. Nat Commun. 2016;7:13317.
18. Agarwal R, Duderstadt KE. Multiplex flow magnetic tweezers reveal rare enzymatic events with single molecule precision. Nat Commun. 2020;11(1):4714.
19. Kah D, Durrbeck C, Schneider W, Fabry B, Gerum RC. High-force magnetic tweezers with hysteresis-free force feedback. Biophys J. 2020;119(1):15–23.
20. Yan J, Skoko D, Marko JF. Near-field-magnetic-tweezer manipulation of single DNA molecules. Phys Rev E Stat Nonlin Soft Matter Phys. 2004;70(1 Pt 1):011905.
21. Pethig R, Markx GH. Applications of dielectrophoresis in biotechnology. Trends Biotechnol. 1997;15(10):426–32.
22. Butt G, Wakeman RJ. Dielectrophoresis as a capture mechanism in filtration. Jubilee Res Event, Two-Day Symp. Rugby, Warwickshire, UK: Institution of Chemical Engineers; 1997. pp. 1073–6.
23. Zhao Y, Hu S, Wang Q. Study on the assembly and separation of biological cell by optically induced dielectrophoretic technology. Microfluid Nanofluid. 2014;17(2):287–94.
24. Yan B, Chen B, Liu FY, Wu JK, Xiong YL. Combining field-modulating electroosmotic vortex and insulating post to manipulate particles based on dielectrophoresis. Appl Math Mech. 2021;42:371–86.
25. Malekanfard A, Beladi-Behbahani S, Tzeng TR, Zhao H, Xuan X. AC insulator-based dielectrophoretic focusing of particles and cells in an “infinite” microchannel. Anal Chem. 2021;93(14):5947–53.
26. Bentor J, Malekanfard A, Raihan MK, Wu S, Pan X, Song Y, et al. Insulator-based dielectrophoretic focusing and trapping of particles in non-Newtonian fluids. Electrophoresis. 2021;42(21–22):2154–61.
27. Bentor J, Raihan MK, McNeely C, Liu Z, Song Y, Xuan X. Fluid rheological effects on streaming dielectrophoresis in a post-array microchannel. Electrophoresis. 2022;43(5–6):717–23.
28. Xuan X. Review of nonlinear electrokinetic flows in insulator-based dielectrophoresis: from induced charge to Joule heating effects. Electrophoresis. 2022;43(1–2):167–89.
29. Chiou PY, Ohta AT, Wu MC. Massively parallel manipulation of single cells and microparticles using optical images. Nature. 2005;436(7049):370–2.
30. Qu YL, Zheng MJ, Liang WF, Dong ZL. Fully automatic wafer-scale micro/nano manipulation based on optically induced dielectrophoresis. Adv Mater Res. 2012;415–417:842–7.
31. Zhu XL, Yin ZF, Gao ZQ, Ni ZH. Experimental study on filtering, transporting, concentrating and focusing of microparticles based on optically induced dielectrophoresis. Sci China Technol Sci. 2010;53(9):2388–96.
32. Hong JL, Yang CM, Chu PY, Chou WP, Liao CJ, Hsieh CH, et al. The effect of operating conditions on the optically induced electrokinetic (OEK)-based manipulation of magnetic microbeads in a microfluidic system. Sens Actuators B. 2019;296:126610.
33. Zhao Y, Hu S, Wang Q. Simulation and analysis of particle trajectory caused by the optical-induced dielectrophoresis force. Microfluid Nanofluid. 2014;16(3):533–40.
34. Liang WF, Liu N, Dong ZL, Liu LQ, Mai JD, Lee GB, et al. Simultaneous separation and concentration of micro- and nanoparticles by optically induced electrokinetics. Sens Actuators A. 2013;193:103–11.
35. Chu PY, Hsieh CH, Lin CR, Wu MH. The effect of optically induced dielectrophoresis (ODEP)-based cell manipulation in a microfluidic system on the properties of biological cells. Biosensors. 2020;10(6):65.
36. Chiu T-K, Chao AC, Chou W-P, Liao C-J, Wang H-M, Chang J-H, et al. Optically-induced-dielectrophoresis (ODEP)-based cell manipulation in a microfluidic system for high-purity isolation of integral circulating tumor cell (CTC) clusters based on their size characteristics. Sens Actuators B. 2018;258:1161–73.
37. Wang H-Y, Chen C-Y, Chu P-Y, Zhu Y-X, Hsieh C-H, Lu J-J, et al. Application of an optically induced dielectrophoresis (ODEP)-based microfluidic system for the detection and isolation of bacteria with heterogeneity of antibiotic susceptibility. Sens Actuators B. 2020;307:127540.
38. Xie SX, Wang XD, Jiao ND, Tung S, Liu LQ. Programmable micrometer-sized motor array based on live cells. Lab Chip. 2017;17(12):2046–53.
39. Chen YS, Chung KC, Huang WY, Lee WB, Fu CY, Wang CH, et al. Generating digital drug cocktails via optical manipulation of drug-containing particles and photo-patterning of hydrogels. Lab Chip. 2019;19(10):1764–71.
40. Chu PY, Liao CJ, Hsieh CH, Wang HM, Chou WP, Chen PH, et al. Utilization of optically induced dielectrophoresis in a microfluidic system for sorting and isolation of cells with varied degree of viability: demonstration of the sorting and isolation of drug-treated cancer cells with various degrees of anti-cancer drug resistance gene expression. Sens Actuators B. 2019;283:621–31.
41. Wang X, Wang X-B, Gascoyne PRC. General expressions for dielectrophoretic force and electrorotational torque derived using the Maxwell stress tensor method. J Electrostat. 1997;39(4):277–95.
42. Ai Y, Qian S. DC dielectrophoretic particle–particle interactions and their relative motions. J Colloid Interface Sci. 2010;346(2):448–54.
43. Hu HH, Patankar NA, Zhu MY. Direct numerical simulations of fluid–solid systems using the arbitrary Lagrangian–Eulerian technique. J Comput Phys. 2001;169(2):427–62.

44. Al Quddus N, Moussa WA, Bhattacharjee S. Motion of a spherical particle in a cylindrical channel using arbitrary Lagrangian–Eulerian method. J Colloid Interface Sci. 2008;317(2):620–30.
45. Zhou T, Ge J, Shi L, Fan J, Liu Z, Woo Joo S. Dielectrophoretic choking phenomenon of a deformable particle in a converging-diverging microchannel. Electrophoresis. 2018;39(4):590–6.
46. Zhou T, Deng Y, Zhao H, Zhang X, Shi L, Woo Joo S. The mechanism of size-based particle separation by dielectrophoresis in the viscoelastic flows. J Fluids Eng. 2018;140(9):091302.
47. Zhou T, Ji X, Shi L, Zhang X, Song Y, Joo SW. AC dielectrophoretic deformable particle-particle interactions and their relative motions. Electrophoresis. 2020;41(10–11):952–8.
48. Zhou T, Ji X, Shi L, Hu N, Li T. Dielectrophoretic interactions of two rod-shaped deformable particles under DC electric field. Colloids Surf A. 2020;607:125493.
49. Shi L, Shi X, Zhou T, Liu Z, Liu Z, Joo S. A full-scale computational study on the electrodynamics of a rigid particle in an optically induced dielectrophoresis chip. Mod Phys Lett B. 2020;34(22):2050233.
50. Shi L, Zhong X, Ding H, Yu Z, Jin J, Zhou T, et al. Continuous separation of microparticles based on optically induced dielectrophoresis. Microfluid Nanofluid. 2022;26(1):6.
51. Liang W, Liu N, Dong Z, Liu L, Mai JD, Lee G-B, et al. Simultaneous separation and concentration of micro- and nanoparticles by optically induced electrokinetics. Sens Actuators A. 2013;193:103–11.
52. Ai Y, Zeng Z, Qian S. Direct numerical simulation of AC dielectrophoretic particle-particle interactive motions. J Colloid Interface Sci. 2014;417:72–79.

SUPPORTING INFORMATION

Additional supporting information can be found online in the Supporting Information section at the end of this article.

How to cite this article: Shi L, Zhong X, Wu T, Bian Q, Liu X, Miao H, et al. The electrodynamics of rod-like microparticles based on optically induced dielectrophoresis. Electrophoresis. 2022;43:2175–2183.
https://doi.org/10.1002/elps.202200102